Low-Temperature Catalytic Pyrolysis of Cellulose in Acidic [Bmim]Otf: A Mechanism Model of Product Evolution

Zhishuncheng Li
Faculty of Environmental Science and Technology,Kunming University of Science and Technology
GuangFei Qu (qgflab@sina.com)
Faculty of Environmental Science and Engineering,Kunming University of Science and Technology
Yanhua He
Faculty of Environmental Science and Engineering,Kunming University of Science and Technology,
Ping Ning
Faculty of Science and Engineering,Kunming University of Science and Technology
Ruosong Xie
Faculty of Science and Engineering,Kunming University of Science and Technology
Weijie Li
Faculty of Science and Engineering,Kunming University of Science and Technology
Yibi Xu
Faculty of Science and Engineering,Kunming University of Science and Technology

Research Article

Keywords: Cellulose, acidic [Bmim]Otf, low-temperature pyrolysis, synergistic catalytic effect, mechanism model

Posted Date: April 27th, 2021

DOI: https://doi.org/10.21203/rs.3.rs-413874/v1

Abstract

In this paper, we studied the catalytic pyrolysis behavior of microcrystalline cellulose (MC) in catalytic systems with acidic [Bmim]OTf as the media at temperatures of 140°C, 180°C, 220°C, 260°C, and 300°C. The pyrolysis behavior was investigated via SEM, XRD, FTIR, and GC-MS. During the catalysis of [Bmim]OTf, the pyrolysis temperature of MC was reduced to 140°C significantly and the crystalline structure of MC was destroyed rapidly. The novel synergistic catalytic effect of $CF_3SO_3^-$ and $[Bmim]^+$ was discovered, which may lead to MC-selective cleavage of glycosidic, C-C, C-O, and C-H bonds, accompanied by new bond formation, which showed the production of many small molecular compounds. Furthermore, a novel mechanism model of evolution in [Bmim]OTf at low temperature was developed from a microscopic point of view. This research had obvious significance for the mechanism of directional regulation of target products, finally realizing the high efficiency utilization of biomass.

1. Introduction

Biomass, the only renewable organic carbon resource in nature, has enormous potential as a replacement for diminishing fossil fuels[1] (Annegret, Martin, Bernd & Klemens, 2012). Cellulose is the most abundant polymer in biomass and is an important material for the production of biofuel and fine chemicals[2] (Huber, Iborra & Corma, 2006). The huge potential market of nano cellulose has been recognized by people, such as reinforced composite materials, shielding film, pigment free color film, pulp and paper additives, concrete reinforcement materials, cosmetics and clinical medicine, nerve cell network scaffold materials, cartilage, tendon repair and other fields are widely favored by the industry, and the trend of nano cellulose entering the commercial market rapidly has been formed[3–4]. At present, nanofibers are also widely used in polymer materials.On the one hand, electrospun nanofibers are often used as templates for inorganic nanofibers and ceramic nanotubes. On the other hand, cellulose and its derivatives are excellent silk polymer matrix for electrospinning[5–7].

Pyrolysis is one of the most important methods for the degradation of cellulose and the production of small molecules that can be burned or chemically transformed[8](You, You, Li & Yong, 2010). However, the existence of intermolecular hydrogen bonds[9](Delarami, Ebrahimi, Bazzi & Khorassani, 2015) and the high chemical stability of glycosidic bonds result in a high pyrolysis temperature (350°C) for cellulose, which is the main bottleneck of cellulose utilization. In this context, many catalysts, such as H_2SO_4, HCl, and H_3PO_4, as well as molecular sieves and metal salts[10–12](Dobele et al., 2005; Hu et al., 2015; Qiang, Wan-Ming, Wen-Zhi, Qing-Xiang & Xi-Feng, 2009) have been developed to produce value-added chemicals and fuel products, with the aim of exploiting the full chemical potential of this currently underutilized but valuable resource[13] (Jiang et al., 2016). However, the application of strong proton acids and sometimes heavy metal salts generally causes serious corrosion and pollution, which is in discordance with the requirements of green chemistry and sustainable development[14] (Chen, 2016).

Ionic liquids (ILs) are a promising class of green and functional solvents. ILs have attracted much attention in recent years, owing to their unusual properties, such as near-zero vapor pressure, high thermal stability, wide electrochemical window, high ionic conductivity and heat capacity, and selective catalytic effect, etc[15–17](Egashira, Asai, Yoshimoto & Morita, 2011; Liu, Cheng, Zhang, Wang & Yu, 2008; Zhang, Grätzel & Hua, 2016). More importantly, ILs can dissolve cellulose[18–19](Hui, Gabriela & Rogers, 2012; Pu, Jiang, Ragauskas & Technology, 2007). The application of ILs as a reaction media can promote reaction efficiency by dissolving the cellulosic macromolecules and thus improving the accessibility of targeted bonds for catalysts, which has become an interesting research topic in the field of ILs for the conversion of cellulose to fuel products or value-added chemicals. Long et al. [20](Long, Li, Guo, Wang, Yu & Wang, 2012) built a novel and efficient cooperative IL pair system for the low-temperature catalytic conversion of cellulose, which was constructed using a combination of an acidic IL catalyst and a cellulose soluble IL solvent, and found that stronger acidity resulted in a lower decomposition temperature and higher solubility of cellulose. DU et al [21](Jun, Liu, Liu, Sun, Tao & Technology, 2010). used 1-butyl-3-methylimidazolium chloride and 1-butyl-3-methylimidazolium tetrafluoroborate as catalysts, and with microwave heating for 20 min, the bio-oil yield from rice straw reached 38% and from sawdust 34%. Liu et al. [22](Liu & Chen, 2006) found that the higher electronegativity of Cl^- is a key ion, which results in a stronger hydrogen bond interaction (O–H···Cl) with the hydroxyl on the side chain of cellulose molecules in [Bmim]Cl. Intramolecular and intermolecular hydrogen bonds of cellulose were effectively destroyed, and the crystallinity of cellulose decreased. According to recent research [23–27](Amarasekara, Owereh & Research, 2009; Changzhi, Qian, ZHAO & Zongbao, 2008; Jiang, Zhu, Ma, Liu & Han, 2011; Liu, Xiao, Xia & Ma, 2013; Zhuo, Du, Bai, Wang, Chen & Wang, 2015), some functionalized ILs can dissolve and pyrolyze cellulose at low temperature. It has been confirmed that IL not only can dissolve cellulose and play a role as a heat medium, but can also exhibit homogeneous catalytic activity and selective catalytic cleavage of various chemical bonds of cellulose in different temperature ranges. Although there are some studies on the pyrolysis process and mechanism of cellulose[28–29](Lédé & Pyrolysis, 2012; Zhu, Zhu, Xiao, Yi & Pyrolysis, 2012)the process and mechanism of pyrolysis is still not completely clear[30–31](Sánchez-Jiménez, Pérez-Maqueda, Perejón & Criado, 2013; Zhang, Song & Han, 2017) and the thermal stability of most ILs is not high. Herein, we used the acidic IL [Bmim]OTf, which has high thermal stability (thermal decomposition temperature more than 400°C), as the reaction medium and cellulose dimer as the basic unit of the catalytic pyrolysis process. The mechanism model of cellulose pyrolysis product evolution at different temperatures was the focus of this study.

2. Experimental Section

2.1. Materials

Microcrystalline cellulose powder (particle size: 50 μm), 1-methylimidazole (purity ≥ 99%), potassium trifluoromethanesulfonate (purity: 98%), 1-chlorobutane (purity ≥ 98%), ethyl acetate (AR, 99%), and dichloromethane (AR, 99.5%) were purchased from Aladdin Reagent.

2.2. Analytical methods

Biochar produced from catalytic pyrolysis of cellulose was characterized via scanning electron microscopy (SEM) (EVO10, Carl Zeiss NTS GmbH, Oberkochen, Germany), X-ray diffraction (XRD) (TD2500 type, Dandong Fang Yuan Instrument Co. Ltd.), and Fourier transform infrared spectroscopy (FTIR) (Tensor 27, Bruker Optics, Germany). Bio-oil was characterized using gas chromatography-mass spectrometry (GC-MS) (GCMSD5975, Agilent).

2.3. Preparation of acidic [Bmim]OTf

Two-step synthesis of acidic [Bmim]OTf specific operations is as follows:

 The synthesis of [Bmim]Cl: 1-chlorobutane and 1-methylimidazole were mixed at a molar ratio of 1.5:1 in a dry 250 mL round-bottomed flask fitted with a condensing tube and stirred for 48 h at 70 °C. When the two phases formed, the top phase, which contained the reagents, was removed by washing several times with ethyl acetate. The yellowish IL product of [Bmim]Cl was further heated up to 80 °C under vacuum to eliminate traces of the ethyl acetate solvent[32] (Huddleston, Visser, Reichert, Willauer, Broker & Rogers, 2001).

 The synthesis of [Bmim]OTf: Potassium trifluoromethanesulfonate and [Bmim]Cl were mixed at a molar ratio of 1:1 in a dry 250 mL round-bottomed flask fitted with a condensing tube, using dichloromethane as the solvent, for reflux condensation for 48 h at 60 °C. After removing the dichloromethane via reduced pressure distillation at 40 °C, the milky and viscous liquid acidic [Bmim]OTf finally was obtained .After that, ethyl acetate was used to clean the milky white viscous liquid [Bmim]OTf,the excess solvent and the potassium chloride generated by the reaction were removed[33]. (Qu, He, Cai, Huang & Ning, 2016).

2.4. Catalytic pyrolysis of MC in acidic [Bmim]OTf

Firstly, the temperature of the heating device was set (140 °C, 180 °C, 220 °C, 260 °C, or 300 °C), then 1.000 g of microcrystalline cellulose and 10.000 g [Bmim]OTf were added into the reactor with a magnetic stirrer for 2 h. During the pyrolysis, the biogas was collected in an aluminum foil bag through the condensing unit. When the pyrolysis reaction finished and the reactor was cooled to room temperature, deionized water and dichloromethane were added to the reactor, and the resultant mixture was filtered to get biochar. The water in the filtrate was removed through the separatory funnel and the dichloromethane evaporated at 40 °C, thus the bio-oil finally was obtained. The catalytic pyrolysis system of microcrystalline cellulose is shown in **Figure 1**.

3. Results And Discussion

3.1. SEM Analysis

SEM images of the MC and biochar at different pyrolysis temperatures are compared in **Figure 2**. The MC has a smooth surface, compact structure, and independent and complete fibers. Under the catalysis of

acidic [Bmim]OTf, the surface of the biochar changed significantly. The surface of the biochar at 140 °C was rough with some folds and holes present, but the biochar still had independent structure, whereas at 180 °C, it was rough with more folds and obvious holes, thinner fibers, distortion, and breakage. When volatiles were released from the melted surface as bursting bubbles, they likely formed obvious pores on the surface[34] (Yu, Paterson, Blamey & Millan, 2016). A large number of crystals were formed on the surface of the biochar at 220 °C, whereas at 260 °C, the crystals had fallen off, and the falling crystals re-polymerized. The biochar at 300 °C, owing to the high degree of devolatilization during the pyrolysis, had a looser and more disordered structure, thus the cellulose broke into small pieces. These phenomena showed that the acidic [Bmim]OTf has an obvious catalytic effect on cellulose pyrolysis, which can significantly reduce the pyrolysis temperature of MC to 140 °C, and the structure of cellulose was severely damaged at low temperature.

3.2. XRD Analysis

The X-ray diffraction model is Dandong Diffractometer Factory TD2500. All data were corrected by subtracting background due to the air scatter and sample holder then we use the fitting program to analyze the pseudo-voigt peak shape.

The crystallinity of cellulose mainly affected the mechanical properties and quality. As the crystallinity of cellulose increased, the tensile strength, hardness, and stability were enhanced, while the hygroscopicity, accessibility, and reactivity decreased [36](Mortazavi, Moghaddam & Polymers, 2010). Because of the fundamental problems with the Segal's methods[37] The crystallinity of the cellulose was determined in terms of the crystallinity index (CrI) according to the **Equation (1)**:

$$CrI = \frac{A_{cryst}}{A_{cryst}+A_{amorph}} \times 100\% \qquad (1)$$

Where A_{cryst} is the area under the calculated pattern for crystalline cellulose and A_{amorph} is the area under the pattern calculated for the amorphous content. The CrI values are listed in Table 1. The XRD patterns of the MC and biochar at different pyrolysis temperatures in [Bmim]OTf are shown in **Figure 3**.

Table 1. CrI values of the cellulose before and after pyrolysis

Sample	MC	Bio-char				
		140 °C	180 °C	220 °C	260 °C	300 °C
CrI value	84.43	67.97	69.4	15.70	10.50	35.51

Compared to the MC (79.6%), the CrI values of biochar (**Table 1**) were significantly lower, which indicated that the acid [Bmim]OTf has good depolymerization property for cellulose, the cellulose molecular chain was broken, and the crystalline region was destroyed. At 140 °C, the biochar showed new diffraction

peaks at 28.6^{o} and 40.8^{o} and the crystallinity decreased to 67.97%, which means the crystalline region of cellulose was destroyed and the crystal structure changed, whereas, at 180 °C, the crystallinity increased to 69.40% and no new diffraction peaks appeared. At 220 °C, the crystallinity of cellulose decreased sharply to 15.70%. Combined with SEM figure, it can be seen that under the catalysis of ionic liquid, the original smooth and independent structure of cellulose becomes rough, and scales appear on the surface of cellulose. With a small amount of shedding, the fiber has gradually peeled off and broken.At the same time, the pyrolysis composition in the liquid phase increased significantly, indicating that cellulose was being decomposed into small molecular bio oil, The reason for this finding might be that the regular hydrogen bonds in cellulose molecules were severely damaged and the crystalline region may have been affected. At 260 ℃, the marker peak of cellulose could not be detected. At this time, several sharp absorption peaks appeared on the X-ray diffraction pattern of biochar, which indicated that the crystalline region of cellulose changed greatly. It can be seen from SEM, the complete structure of cellulose can not be seen in the figure, and almost all of them are decomposed into small molecular aggregates. At the same time, the most liquid phase components are detected at 260 ℃, indicating that the cellulose is completely decomposed at this temperature.The biochar crystalline and amorphous regions of the diffraction peak intensity significantly increased at 300 °C, but the crystallinity decreased to 35.51%. Moreover, SEM shows that there is a relatively complete cellulose structure in the figure below, which is different from 260 ℃, and only three substances were detected in GC-MS detection, which indicates that the cellulose cracking at this temperature was not as complete as that at 260 ℃, which may be due to the partial deactivation of ionic liquid at this temperature, resulting in the loss of part of the catalysis of ionic liquid The decomposition of cellulose is not complete at this temperature.

3.3. FTIR Analysis

FTIR spectra of the biochar at different pyrolysis temperatures were compared with those of the MC, as is shown in **Figure 4**. The infrared absorption peak position of biochar at 180 °C was the same as that of MC, but new absorption peaks appeared at 140 °C, 220 °C, 260 °C, and 300 °C. The intramolecular hydroxyl (O-H) stretching vibration of MC at 3336 cm^{-1} [38-39](Bordoloi, Narzari, Chutia, Bhaskar & Kataki, 2015; Fan et al., 2013), broadening and shifting to lower frequency, indicated that many hydrogen bonds were present in the cellulose molecules. The peak observed around 2893 cm^{-1} was due to C-H stretching vibration[40] (Melo et al., 2009). The characteristic absorption band at 1035 cm^{-1} was designated the sugar C-OH stretching peak.

Compared with the infrared absorption peak of the MC, the absorption bands of the biochar at 3336 cm^{-1} (O-H) and 1035 cm^{-1} (C-OH) increased at 140 °C, which indicates that the hydrogen-bonded network structure of cellulose was destroyed and there was interference of the saccharide hydroxyl groups. At 220 °C and 260 °C, the absorption bands at 3329 cm^{-1} (O-H) and 2880 cm^{-1} (C-H) were obviously weaker or even absent, indicating that the dehydration reaction of cellulose molecules lost numerous hydroxyl groups. New absorption peaks were present at 2977 cm^{-1}, 2360 cm^{-1}, 1557 cm^{-1}, 1251 cm^{-1}, 1155 cm^{-1}, 842 cm^{-1}, and 759 cm^{-1}. The peak at 2977 cm^{-1} was ascribed to olefin CH_2 symmetric stretching, which

signifies the presence of olefins. The 2360 cm^{-1} peak was attributed to antisymmetric stretching of CO_2, indicating the decarbonylation of acids and aldehydes resulting in decomposition to CO_2. The peak at 1557 cm^{-1} was for COO^- antisymmetric stretching, which indicates that small molecules containing carboxylic acid were produced after cellulose fracturing. The 1251 cm^{-1} peak was due to cyclic anhydride C-O-C antisymmetric stretching [41](Mohammed, Abakr, Kazi, Yusup, Alshareef & Chin, 2015), which may have formed substances of cyclic anhydride structure. The peaks at 1155 cm^{-1} belong to C=O stretching vibrations in the ester group of the carbonyl [42](Schwanninger, Rodrigues, Pereira & Hinterstoisser, 2004), whereas the peaks at 759 cm^{-1} and 842 cm^{-1} were ascribed to C-H stretching vibration in aromatic structures [43-44](Yi-Hu, Yang, Xin, Liu & Dong, 2013; Yorgun, Yıldız & Pyrolysis, 2015). As the pyrolysis temperature increased, new infrared absorption peaks appeared for the biochar, which was mainly from the presence of [Bmim]OTf and the increase of temperature, which accelerates the depolymerization of cellulose.

3.4. GC-MS Analysis of the Bio-oil

The acidic [Bmim]OTf used in this study has a strong catalytic effect on cellulose pyrolysis, and the cellulose can be decomposed into numerous small molecular compounds at low temperature. GC-MS analysis showed that the bio-oil consisted mainly of alcohols, acids, esters, ketones, etc. The chemical structures of the main identified compounds of the bio-oil are presented in **Table 2**.

Table 2. Main components of the bio-oil at different pyrolysis temperatures

Bio-oil composition	Molecular Structure	Pyrolysis Temperature				
		140 °C	180 °C	220 °C	260 °C	300 °C
furfuryl alcohol $C_5H_6O_2$	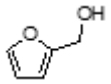	√	√	√		√
3-pentanol $C_5H_{14}O$	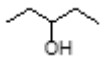		√	√		
1,4-butyrolactone $C_4H_6O_2$			√	√	√	√
vinyl propionate $C_5H_8O_2$	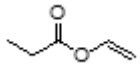				√	
4-hydroxybutanoic acid $C_4H_8O_3$	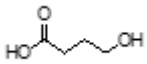		√	√	√	√
succinic anhydride $C_4H_4O_3$				√		
5-methylfurfural $C_6H_6O_2$	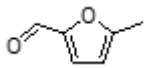		√			
2-oxobutyl acetate $C_6H_{10}O_3$	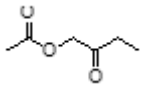				√	
4-methyl-2(5H)-furanone $C_5H_6O_2$	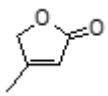				√	
alpha-methyl-gamma-butyrolactone $C_5H_8O_2$;					√	

3.5. FTIR Analysis the Mechanism Model of Bio-oil Evolution in [Bmim]OTf

Generally, the components of bio-oil have wide distribution, low content, and poor stability in conventional thermal chemical techniques for cellulose utilization, thus it is difficult to get high-level use directly. Therefore, this study on the mechanism of low-temperature catalytic pyrolysis of cellulose in [Bmim]OTf

was conducted to control the pyrolysis process and optimize the pyrolysis products. In general, during cellulose pyrolysis, the hydrolysis reaction proceeds first, generating glucose monomers and other small molecular compounds [45](Shen & Gu, 2009). In this study, [Bmim]OTf was used as a catalyst and reaction medium, and cellulose dimer was regarded as the basic unit to study the mechanism model of bio-oil evolution in [Bmim]OTf. The first step was to catalyze the hydrolysis of the glycosidic bond of the cellulose dimer via [Bmim]OTf and form glucose monomers. Then, the glucose monomers can generate many small molecular compounds through pyrolysis at low temperature.

The key to analyze the pyrolysis process of cellulose dimer is to obtain the charge distribution on each chemical bond, and then reasonably infer the reaction path of cellulose dimer pyrolysis based on GC / MS spectrum. Through Mulliken population analysis [46], we can calculate the value of charge distribution. However, this analysis method is too dependent on the calculated basis set, and sometimes the calculation will result in negative numbers without physical significance.In contrast, the natural bond orbit method (NBO) [47] has a great advantage: even when the calculated basis set changes, the calculated value has better stability, and it is suitable for both classic ab initio calculations in the DFT method. Therefore, NBO is widely used in theoretical chemical bond formation research. The NBO charge population of the cellulose dimer is shown in Table 3. At low temperature, the cation and anion synergistic catalysis breaks the glycosidic bond of the cellulose dimer, and the molecular mechanism of such is shown in **Figure** 5.

Table 3. The bond NBO charge population of the cellulose dimer.

Bond	Bond lengths(Å)	NBO charge population	Bond	Bond lengths(Å)	NBO charge population
C_1 — C_2	1.5365	0.9745	C_2 — O_{19}	1.4108	0.9261
C_2 — C_3	1.5412	0.9749	C_3 — O_{18}	1.4394	0.9076
C_3 — C_4	1.5325	0.9887	C_4 — O_{17}	1.4184	0.9195
C_4 — C_5	1.5401	0.9697	C_1 — O_8	1.4136	0.8363
C_5 — C_6	1.5219	1.0054	C_1 — O_7	1.4148	0.9020
C_5 — O_7	1.4405	0.8621	C_9 — O_8	1.4417	0.8924

The numbers of NBO charge populations for C_1-O_8 and C_9-O_8 were 0.8363 and 0. 8924 (**Table 3**), respectively, so the C_1-O_8 bond was easier to break than the C_9-O_8 bond during pyrolysis. The $[Bmim]^+$ was used as a Brφnsted acid to protonate the glycosic oxygen (O_8) in the low-temperature catalytic pyrolysis system of cellulose. The $CF_3SO_3^-$ acted as a nucleophile to attack the anomeric carbon C_1 of the cellulose dimer, thus the glycosidic bond was broken under the synergistic catalysis effect of the anionic $CF_3SO_3^-$ and cationic $[Bmim]^+$. Then, the hydroxyl groups of the water molecules attacked the anomeric carbon C_1, which led to $CF_3SO_3^-$ away from anomeric carbon C_1, and the cation as Brφnsted base to accept H^+ in water molecular, thus the Brφnsted acid $[Bmim]^+$ was regenerated. Finally, the $[Bmim]^+$ and $CF_3SO_3^-$ were involved in cyclic reaction of the glycosidic bond hydrolysis. The hydrolysis of the glycosidic bond decreased the crystallinity of the cellulose, increased the contact area between [Bmim]OTf and the cellulose, and promoted the catalytic pyrolysis reaction. The mechanism model of furfuryl alcohol and 5-methylfurfural from bio-oil evolution in [Bmim]OTf is shown in **Figure 6**, whereas that of 4-hydroxybutanoic acid and 1,4-butyrolactone is shown in **Figure 7**.

The $[Bmim]^+$ protonated the O_7 and the $CF_3SO_3^-$, as a nucleophile, tended to attack the C_1. The C_1-O_7 bond (NBO charge population was 0.9020) was fractured under the synergistic catalysis effect of the anions and cations at temperatures ≥ 140 °C. Meanwhile, the C_1 participated in the carbonylation reaction after the -O_{24}H released H^+. Under the catalysis of the IL, the C_2-C_3 dehydrated to generate an enol structure, and this unstable enol structure experienced rearrangement to form a ketone carbonyl (C_2=O). Polymerization occurred between the C_2=O and C_5-OH, and then dehydration produced 5-hydroxymethyl furfural. The $[Bmim]^+$ protonated the O_{24}, and 2-furfuryl alcohol was derived from decarbonylation of the 5-hydroxymethyl furfural after the hydrogen bond formed via $CF_3SO_3^-$ and H^+ of the C_1. The -O_{16}H was protonated by $[Bmim]^+$, then dehydrated to produce 5-methylfurfural at 180 °C.

The length of the C_2-C_3 bond in the pyranoglucose molecule was longer than that of the other C-C bonds; as a result, the C_2-C_3 was more likely to break[48](Shen, Jin, Hu, Xiao & Luo, 2015). When the pyrolysis temperature was ≥ 180 °C, the $[Bmim]^+$ protonated the O_7 and a hydrogen bond formed via $CF_3SO_3^-$ with H^+ of the C_1 and -OH. Meanwhile, the glucopyranose molecule absorbed heat, which leading to the intensification of the atomic motion and the elongation of atomic bond . Subsequently, the stability of the C_2-C_3 bond and C_1-O_7 bond of the hemiacetal was destroyed, along with the break of glucopyranose ring. This resulted in the formation of a four-carbon fragment and a two-carbon fragment. The two-carbon fragment was extremely unstable and thus was reorganized to the relatively stable glycolaldehyde. The $[Bmim]^+$ protonated the -O_7H from the four-carbon fragment by removing one molecule of H_2O. Meanwhile, a ketene structure was produced via C_3-C_4 dehydration. Because the ketene structure was very unstable, 4-hydroxybutyric acid was formed via addition reaction of the ketene with water. Furthermore, 1,4-butyrolactone evolved through C_3-C_6 condensation.

Only representative portions of the mechanism model of bio-oil evolution in [Bmim]OTf are listed above. In the absence of [Bmim]OTf, the initial decomposition temperature of cellulose is 350 °C, but acidic [Bmim]OTf can significantly reduced the pyrolysis temperature of cellulose to 140 °C and generated numerous small molecular compounds with high added value. This may be due to the introduction of acidic [Bmim]OTf, which promotes the heat transfer efficiency during the pyrolysis process. Furthermore, the anions and cations synergistic catalyzed the selective cleavage of glycosidic bond and other chemical bonds of cellulose.

4. Conclusions

An efficient and stable [Bmim]OTf was prepared for the selective catalytic pyrolysis of MC, which significantly reduced the pyrolysis temperature and rapidly destroyed the crystalline structure of MC. Based on this study of the mechanism of $[Bmim]^+$ and $CF_3SO_3^-$ synergistic catalytic pyrolysis of the cellulose dimer, a mechanism model of product evolution was obtained. With the synergistic catalysis effect of $[Bmim]^+$ and $CF_3SO_3^-$, numerous small molecular compounds with high added value such as alcohols, acids, esters, ketones, and aldehydes were produced through a series of reactions such as dehydration, rearrangement, decarbonylation, and condensation.

Declarations

Acknowledgements

The authors greatly acknowledge the funding support of the National Natural Science Foundation of China (No. 2018YFC0213403).

Declaration of interest statement

We declare that we have no financial and personal relationships with other people or organizations that can inappropriately influnce our work,there is no professional or other interest of a nature or kind in any product,service and/or company that could be construed as influencing the position in the manuscript entitled.

We declare that all experiments and operations in this article are conducted in accordance with humanitarian and ethical principles.

References

1. Annegret, Stark, Martin, Sellin, Bernd, & Ondruschka, et al. (2012). The effect of hydrogen bond acceptor properties of ionic liquids on their cellulose solubility. Science China Chemistry. https://doi.org/10.1007/s11426-012-4685-8
2. George, W., Huber, Sara, Iborra, & Avelino, et al. (2006). Synthesis of transportation fuels from biomass: chemistry, catalysts,and engineering. ChemInform.

https://doi.org/10.1002/chin.200652240

3. Lindstrm, Aulin. Market and technical challenges and opportunities in the area of innovative new materials and composites based on nanocellulosics[J]. Scandinavian Journal of Forest Research, 2014, 29(4):345-351.
4. Wang Q, Yu D G, Zhang L L, et al. Electrospun hypromellose-based hydrophilic composites for rapid dissolution of poorly water-soluble drug[J]. Carbohydrate Polymers, 2017:S0144861717307129. https://doi.org/10.1016/j.carbpol.2017.06.075
5. Liu X, Yang Y, Yu D G, et al. Tunable zero-order drug delivery systems created by modified triaxial electrospinning[J]. Chemical Engineering Journal, 2019, 356:886-894. https://doi.org/10.1016/j.cej.2018.09.096
6. Deng-Guang, Jiao-Jiao, Gareth, R, Williams, Min, & Zhao. (2018). Electrospun amorphous solid dispersions of poorly water-soluble drugs: a review. Journal of controlled release: official journal of the Controlled Release Society. https://doi.org/10.1016/j.jconrel.2018.08.016
7. Zhou H, Shi Z, Wan X, et al. The Relationships between Process Parameters and Polymeric Nanofibers Fabricated Using a Modified Coaxial Electrospinning[J]. Nanomaterials, 2019, 9(6).
8. You, Z. , You, S. , Li, X. , Luo, Y. , & Jiao, Y. . (2010). The Carbonization Characteristics Studies of Corn Stalk in a Fixed Bed Reactor. International Conference on Bioinformatics & Biomedical Engineering. IEEE.
9. Delarami, H. S. , Ebrahimi, A. , Bazzi, S. , & Habibi Khorassani, S. M. . (2015). The effect of intramolecular hydrogen bond on the n-glycosidic bond strength in 3-methyl-2'-deoxyadenosine: a quantum chemical study. Structural Chemistry, 26(2), 411-419. https://doi.org/10.1007/s11224-014-0493-4
10. Dobele, G. , Rossinskaja, G. , Dizhbite, T. , Telysheva, G. , Meier, D. , & Faix, O. . (2005). Application of catalysts for obtaining 1,6-anhydrosaccharides from cellulose and wood by fast pyrolysis. Journal of Analytical & Applied Pyrolysis. https://doi.org/10.1016/j.jaap.2004.11.031
11. Hu, S. , Jiang, L. , Wang, Y. , Su, S. , & Xiang, J. . (2015). Effects of inherent alkali and alkaline earth metallic species on biomass pyrolysis at different temperatures. Bioresource Technology, 192, 23-30. https://doi.org/10.1016/j.biortech.2015.05.042
12. Lu, Q. , Xiong, W. M. , Li, W. Z. , Guo, Q. X. , & Zhu, X. F. . (2009). Catalytic pyrolysis of cellulose with sulfated metal oxides: a promising method for obtaining high yield of light furan compounds. Bioresource Technology, 100(20), 4871-4876. https://doi.org/10.1016/j.biortech.2009.04.068
13. [13]Jiang, Z., Zhang, Z., Song, J., Meng, Q., Zhou, H., He, Z., Han, B. J. A. S. C., & Engineering. (2016). Metal-oxide-catalyzed efficient conversion of cellulose to oxalic acid in alkaline solution under low oxygen pressure. Acs Sustainable Chemistry & Engineering, 4(1), acssuschemeng.5b01212. https://doi.org/10.1021/acssuschemeng.5b01212
14. Chen, Zhengjian, Long, & Jinxing. (2016). Organosolv liquefaction of sugarcane bagasse catalyzed by acidic ionic liquids. Bioresource Technology Biomass Bioenergy Biowastes Conversion Technologies Biotransformations Production Technologies.

15. Egashira, M. , Asai, T. , Yoshimoto, N. , & Morita, M. . (2011). Ionic conductivity of ternary electrolyte containing sodium salt and ionic liquid. Electrochimica Acta, 58(none), 95-98. https://doi.org/10.1016/j.electacta.2011.08.100
16. Liu, W. , Cheng, L. , Zhang, Y. , Huaping Wang, & Yu, M. . (2008). The physical properties of aqueous solution of room-temperature ionic liquids based on imidazolium: database and evaluation. Journal of Molecular Liquids, 140(1-3), 68-72. https://doi.org/10.1016/j.molliq.2008.01.008
17. Zhang, X. , Michael Grätzel, & Hua, J. . (2016). Donor design and modification strategies of metal-free sensitizers for highly-efficient n-type dye-sensitized solar cells. Frontiers of Optoelectronics. https://doi.org/10.1007/s12200-016-0563-x
18. Wang, H. , Gurau, G. , & Rogers, R. D. . (2012). Cheminform abstract: ionic liquid processing of cellulose. Cheminform, 43(19), no-no. https://doi.org/10.1002/chin.201219271
19. Pu, Y. , Jiang, N. , & Ragauskas, A. J. . (2007). Ionic liquid as a green solvent for lignin. Journal of Wood Chemistry & Technology, 27(1), 23-33. https://doi.org/10.1080/02773810701282330
20. Long, J. , Li, X. , Guo, B. , Wang, F. , Yu, Y. , & Wang, L. . (2012). Simultaneous delignification and selective catalytic transformation of agricultural lignocellulose in cooperative ionic liquid pairs. Green Chemistry, 14(7), 1935-1941. https://doi.org/10.1039/c2gc35105f
21. Jun, D. U. , Ping, L. , Dagui, L. Z. , & Changyuan, T. . (0). Support info of fast pyrolysis of biomass for bio-oil with ionic liquid and microwave irradiation. J Fuel Chem Technol.
22. Liying, L. , & Hongzhang, C. . (2006). Enzymatic hydrolysis of cellulose materials treated with ionic liquid [bmim] cl. Chinese Science Bulletin, 51(20), 2432-2436. https://doi.org/10.1007/s11434-006-2134-9
23. Amarasekara, A. S. , & Owereh, O. S. . (2009). Hydrolysis and decomposition of cellulose in brnsted acidic ionic liquids under mild conditions. Industrial & Engineering Chemistry Research, 48(22), 10152-10155. https://doi.org/10.1021/ie901047u
24. Li, C. , Wang, Q. , & Zhao, Z. K. . (2008). Acid in ionic liquid: an efficient system for hydrolysis of lignocellulose. Green Chemistry, 10(2), 177-182. https://doi.org/10.1039/b711512a.
25. Jiang, F. , Zhu, Q. , Ma, D. , Liu, X. , & Han, X. . (2011). Direct conversion and nmr observation of cellulose to glucose and 5-hydroxymethylfurfural (hmf) catalyzed by the acidic ionic liquids. Journal of Molecular Catalysis A Chemical, 334(1-2), 8-12. https://doi.org/10.1016/j.molcata.2010.10.006
26. Liu, Y. , Xiao, W. , Xia, S. , & Ma, P. . (2013). So 3 h-functionalized acidic ionic liquids as catalysts for the hydrolysis of cellulose. Carbohydrate Polymers, 92(1), 218-222. https://doi.org/10.1016/j.carbpol.2012.08.095
27. Bai, Guangyue, Wang, Jianji, Chen, & Yujuan, et al. (2015). Hydrolysis of cellulose catalyzed by novel acidic ionic liquids. Carbohydrate Polymers: Scientific and Technological Aspects of Industrially Important Polysaccharides, 115, 49-53.
28. Jacques Lédé. (2012). Cellulose pyrolysis kinetics: an historical review on the existence and role of intermediate active cellulose. Journal of Analytical and Applied Pyrolysis, 94, 17–32. https://doi.org/10.1016/j.jaap.2011.12.019.

29. Zhu, G. , Zhu, X. , Xiao, Z. , & Yi, F. . (2012). Study of cellulose pyrolysis using an in situ visualization technique and thermogravimetric analyzer. Journal of Analytical & Applied Pyrolysis, 94(Mar.), 126-130. https://doi.org/10.1016/j.jaap.2011.11.016.
30. Sánchez-Jiménez, Pedro E., Pérez-Maqueda, Luis A., Perejón, Antonio, & Criado, José M. (2013). Generalized master plots as a straightforward approach for determining the kinetic model: the case of cellulose pyrolysis. Thermochimica Acta, 552(2), 54-59. https://doi.org/10.1016/j.tca.2012.11.003.
31. Zhanrong, Zhang, Jinliang, Song, Buxing, & Han. (2016). Catalytic transformation of lignocellulose into chemicals and fuel products in ionic liquids. Chem. Rev. https://doi.org/10.1021/acs.chemrev.6b00457
32. Huddleston, J. G. , Visser, A. E. , Reichert, W. M. , Willauer, H. D. , Broker, G. A. , & Rogers, R. D. . (2001). Characterization and comparison of hydrophilic and hydrophobic room temperature ionic liquids incorporating the imidazolium cation. Green Chemistry, 3. https://doi.org/10.1039/B103275P
33. Xi, H. , Guangfei, Q. , Ping, N. , Weiwei, H. , & Yingying, C. . (2016). Catalytic pyrolysis of cellulose in ionic liquid [bmim]otf. Carbohydrate Polymers: Scientific and Technological Aspects of Industrially Important Polysaccharides.
34. Yu, J. , Paterson, N. , Blamey, J. , & Millan, M. . (2016). Cellulose, xylan and lignin interactions during pyrolysis of lignocellulosic biomass. Fuel, 191, 140-149. https://doi.org/10.1016/j.fuel.2016.11.057
35. Coomey, J. H. , & Hazen, S. P. . (2015). Brachypodium distachyon as a Model Species to Understand Grass Cell Walls. Springer International Publishing.
36. Mortazavi, S. M. , & Moghaddam, M. K. . (2010). An analysis of structure and properties of a natural cellulosic fiber (leafiran). Fibers and Polymers, 11(6), 877-882. https://doi.org/10.1007/s12221-010-0877-z
37. [37]Ling Z , Wang T , Makarem M , et al. Effects of ball milling on the structure of cotton cellulose[J]. Cellulose, 2019. https://doi.org/10.1007/s10570-018-02230-x
38. Bordoloi, N. , Narzari, R. , Chutia, R. S. , Bhaskar, T. , & Kataki, R. . (2014). Pyrolysis of mesua ferrea and pongamia glabra seed cover: characterization of bio-oil and its sub-fractions. Bioresource Technology, 178, 83-89. https://doi.org/10.1016/j.biortech.2014.10.079
39. Fan, G. , Liao, C. , Fang, T. , Wang, M. , & Song, G. . (2013). Hydrolysis of cellulose catalyzed by sulfonated poly(styrene-co-divinylbenzene) in the ionic liquid 1-n-butyl-3-methylimidazolium bromide. Fuel Processing Technology, 116, 142-148. https://doi.org/10.1016/j.fuproc.2013.05.009
40. Júlio C.P. de Melo, Filho, E. C. D. S. , Santana, S. A. A. , & Airoldi, C. . (2009). Maleic anhydride incorporated onto cellulose and thermodynamics of cation-exchange process at the solid/liquid interface. Colloids & Surfaces A Physicochemical & Engineering Aspects, 346(1-3), 138-145. https://doi.org/10.1016/j.colsurfa.2009.06.006
41. Mohammed, I. , Abakr, Y. , Kazi, F. , Yusup, S. , Alshareef, I. , & Chin, S. . (2015). Comprehensive characterization of napier grass as a feedstock for thermochemical conversion. Energies, 8(5), 3403-3417. https://doi.org/10.3390/en8053403

42. B, M. S. A. , C, J. C. R. , C, H. P. , & D, B. H. B. . (2004). Effects of short-time vibratory ball milling on the shape of ft-ir spectra of wood and cellulose - sciencedirect. Vibrational Spectroscopy, 36(1), 23-40. https://doi.org/10.1016/j.vibspec.2004.02.003
43. Ke, Y. H. , Yang, E. T. , Liu, X. , Liu, C. L. , & Dong, W. S. . (2013). Preparation of porous carbons from non-metallic fractions of waste printed circuit boards by chemical and physical activation. New Carbon Materials, 60, 563-563. https://doi.org/10.1016/j.carbon.2013.04.024
44. Yorgun, Sait, Yildiz, & Derya. (2015). Slow pyrolysis of paulownia wood: effects of pyrolysis parameters on product yields and bio-oil characterization. Journal of analytical & applied pyrolysis.
45. Shen, D. K. , & Gu, S. . (2009). The mechanism for thermal decomposition of cellulose and its main products. Bioresource Technology, 100(24), 6496-6504. https://doi.org/10.1016/j.biortech.2009.06.095
46. Mulliken, R. S. . (1955). Electronic population analysis on lcao□o molecular wave functions. iii. effects of hybridization on overlap and gross ao populations. The Journal of Chemical Physics, 23(12), 2338-2342. https://doi.org/10.1063/1.1741876
47. Reed, A.E., Curtiss, L.A. and Weinhold, F. (1988) Intermolecular Interactions from a Natural Bond Orbital, Donor-Acceptor Viewpoint. Chemical Review. https://doi.org/10.1021/cr00088a005
48. [48]Shen, D., Jin, W., Hu, J., Xiao, R., & Luo, K. J. C. (2015). An overview on fast pyrolysis of the main constituents in lignocellulosic biomass to valued-added chemicals: structures, pathways and interactions. Cheminform, 51, 761-774. https://doi.org/10.1016/j.rser.2015.06.054

Figures

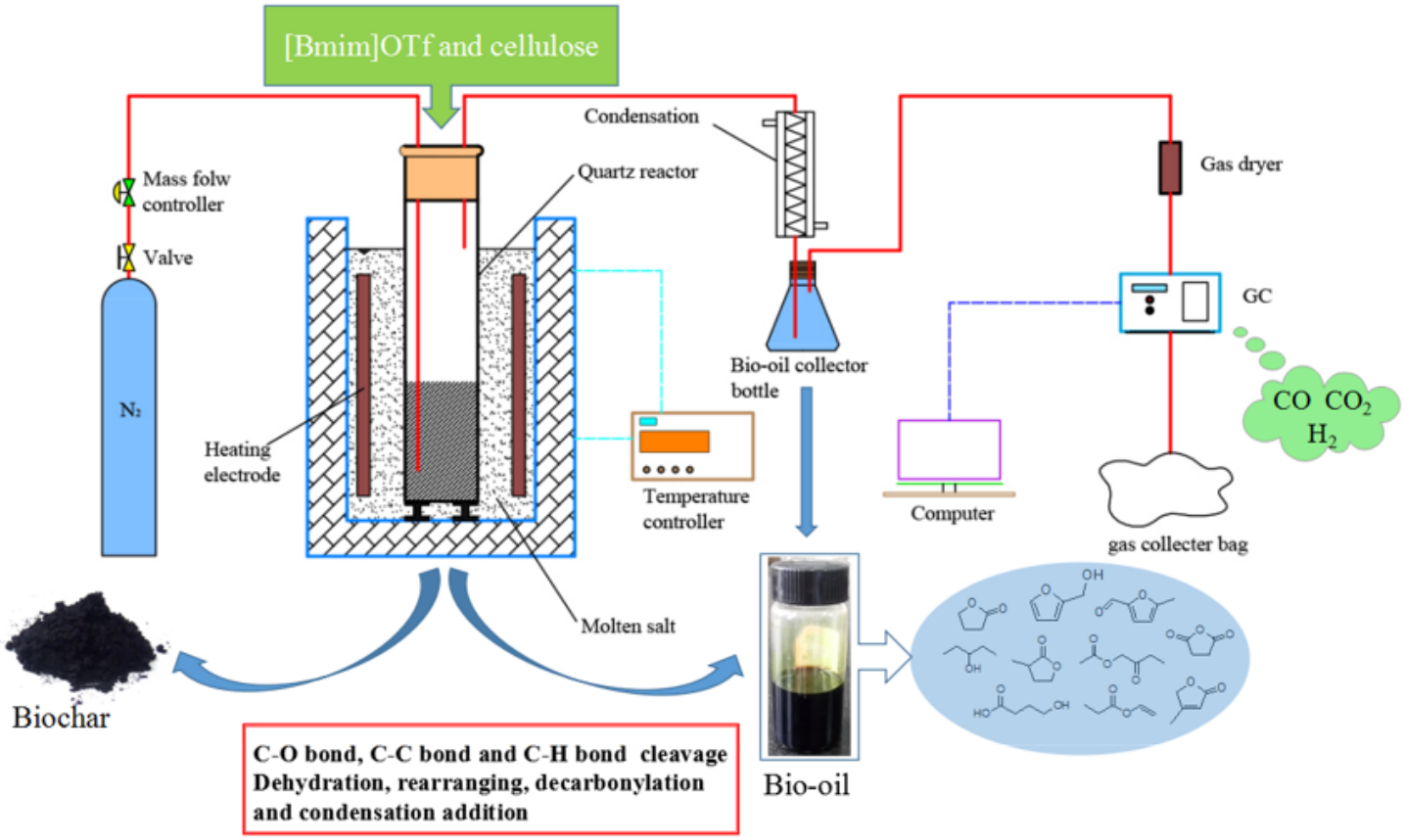

Figure 1

Catalytic pyrolysis system of MC in acidic [Bmim]OTf.

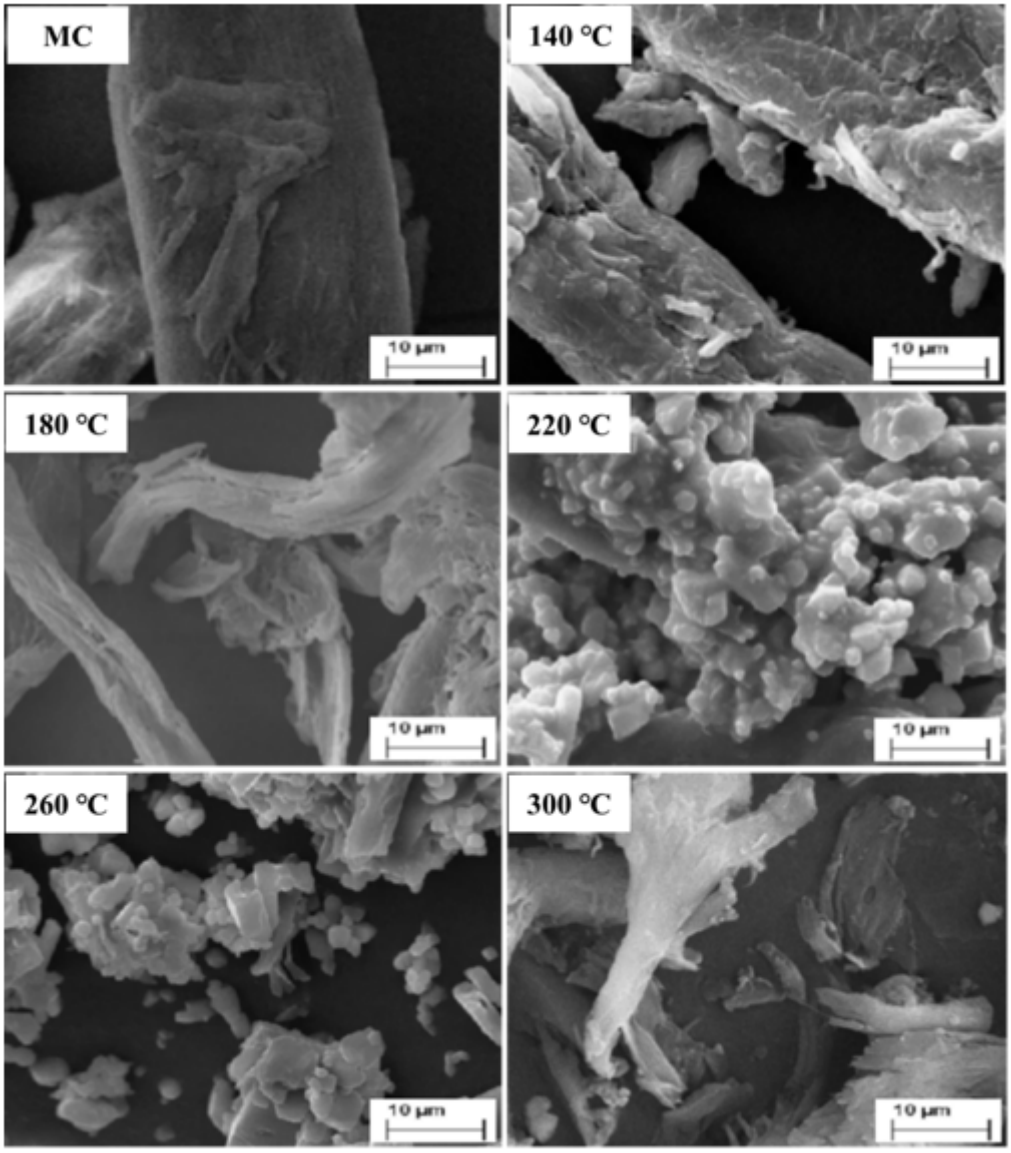

Figure 2

SEM images of MC and biochar at different pyrolysis temperatures.

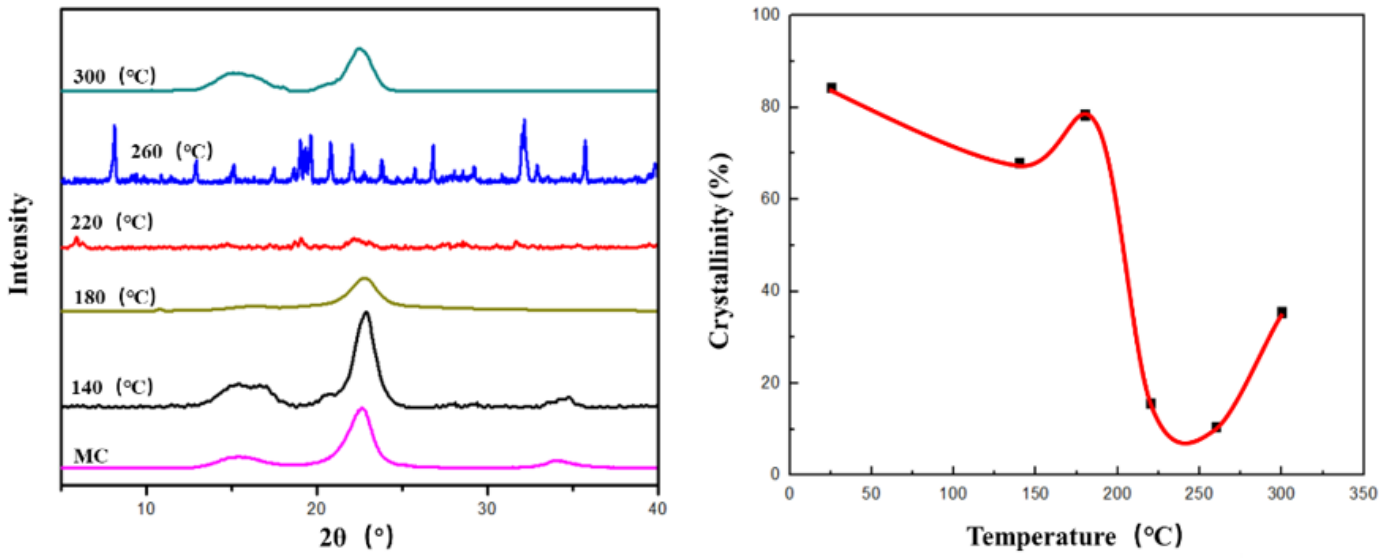

Figure 3

XRD analysis of the MC and biochar at different pyrolysis temperatures. a: XRD patterns; b: FTIR spectra.

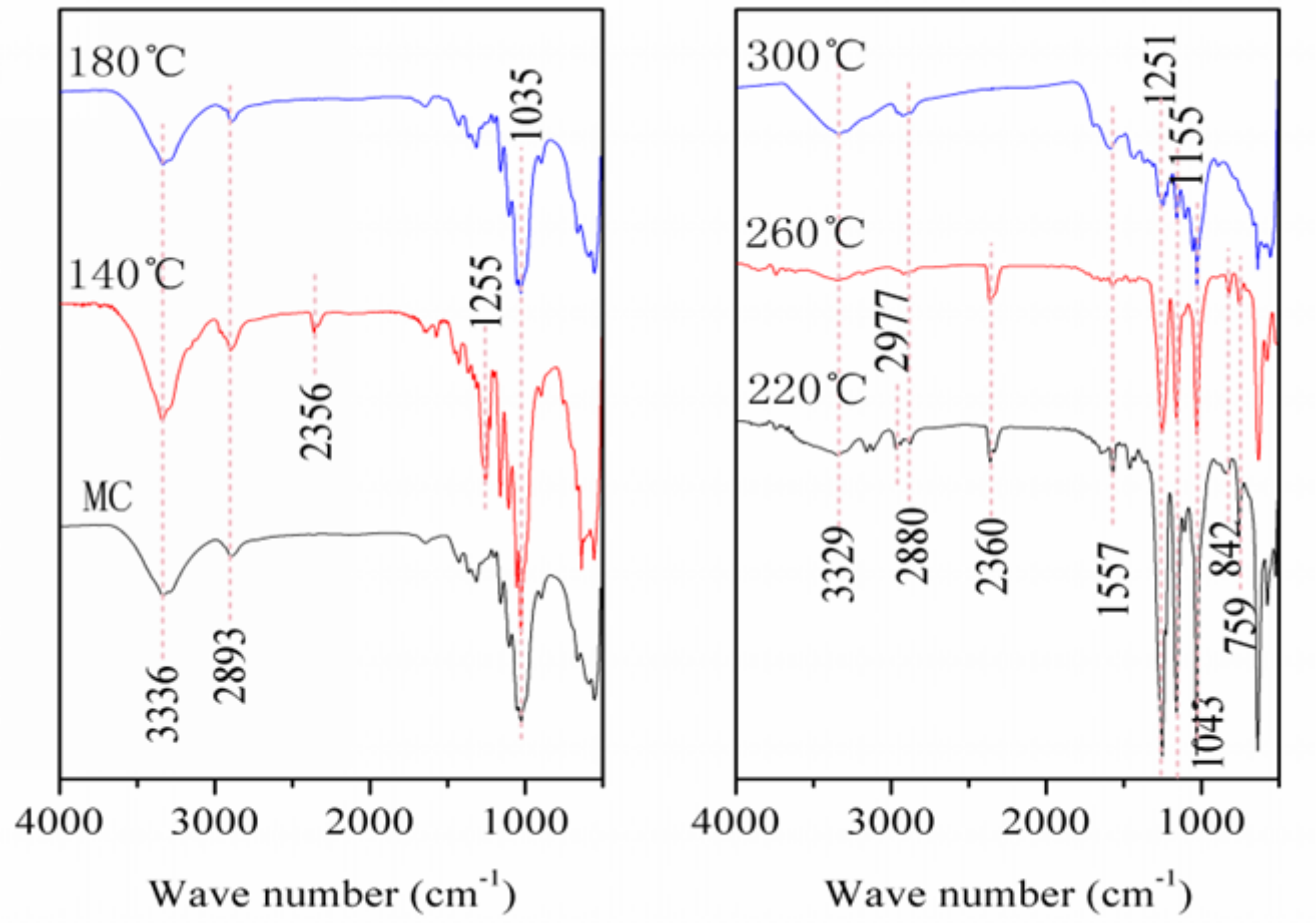

Figure 4

FTIR analysis of the MC and biochar at different pyrolysis temperatures.

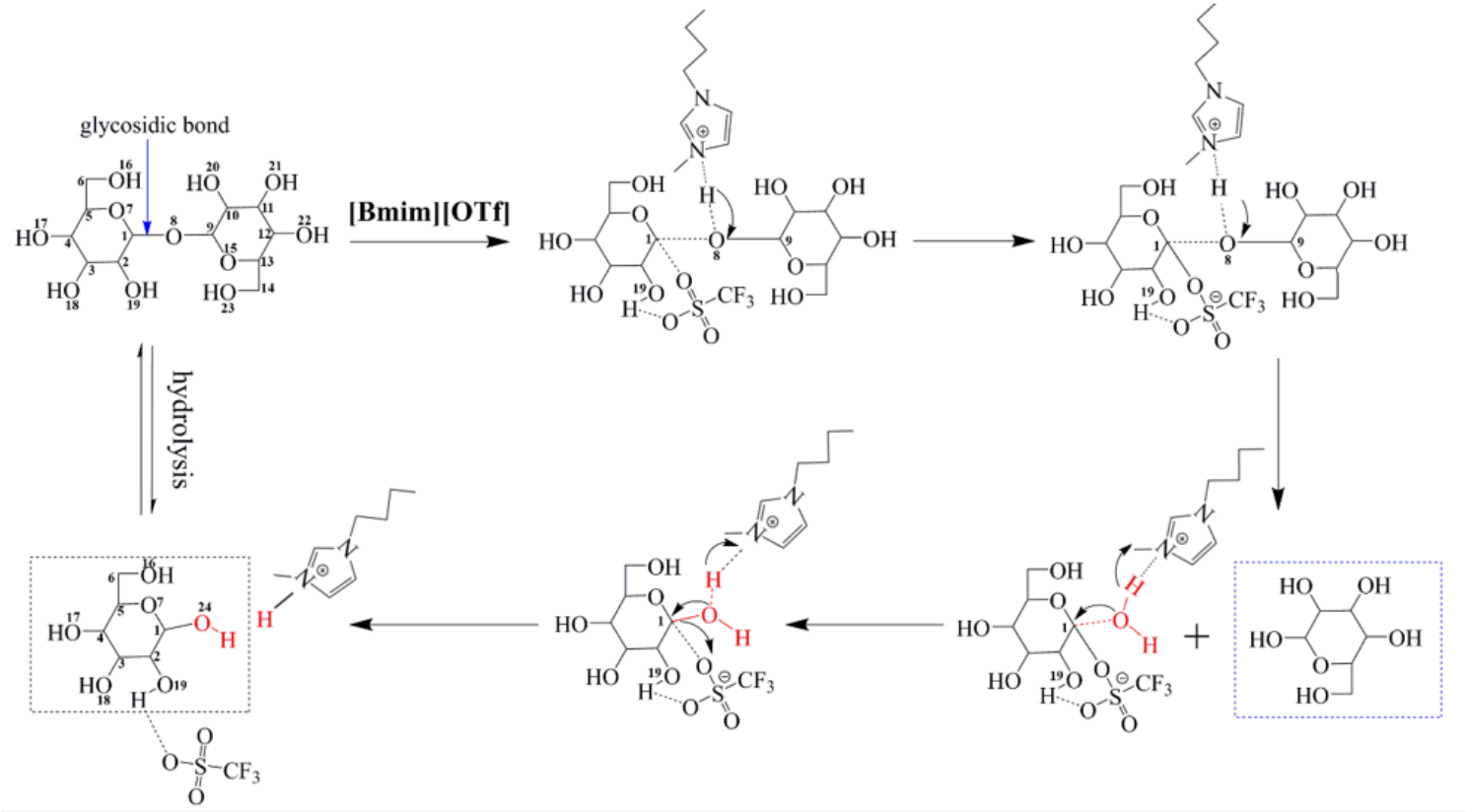

Figure 5

Molecular mechanism of the [Bmim]OTf-catalyzed glycosidic bond cleavage.

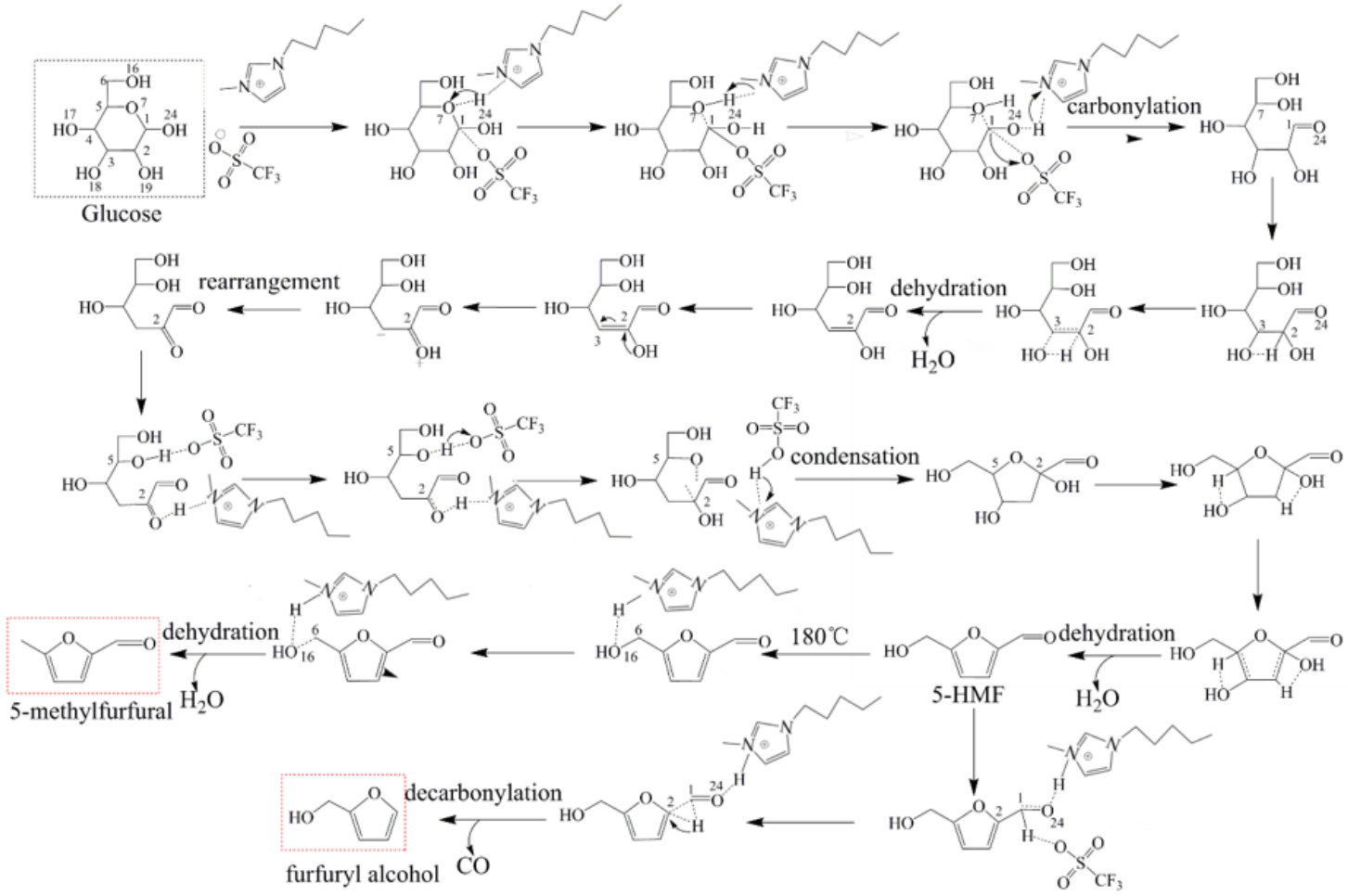

Figure 6

The mechanism model of furfuryl alcohol and 5-methylfurfural evolution in [Bmim]OTf.

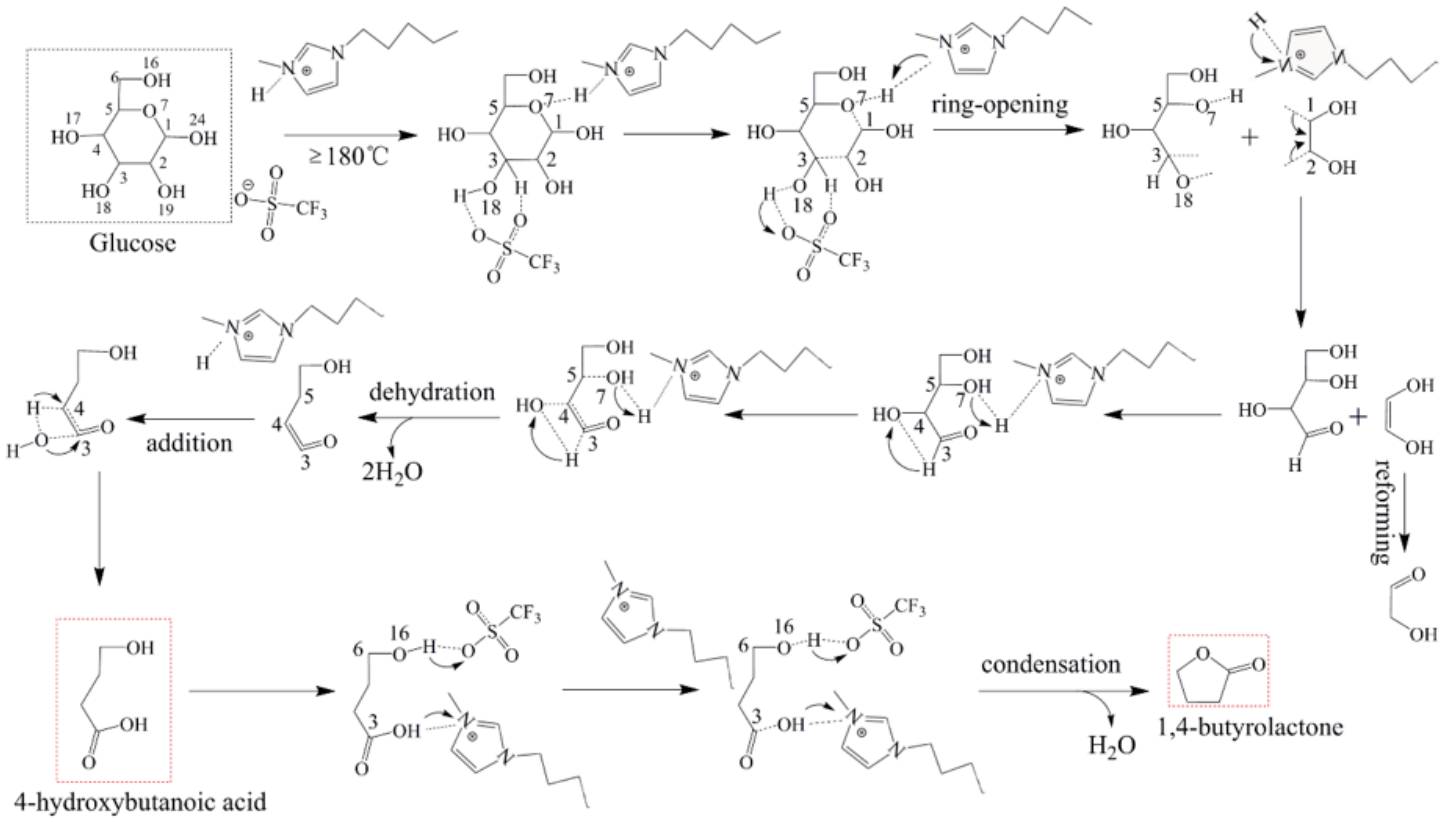

Figure 7

The mechanism model of 4-hydroxybutanoic acid and 1,4-butyrolactone evolution in [Bmim]OTf.